## Abstract

The design and synthesis of novel electron-deficient and solution-processable polycyclic aromatic hydrocarbons offers great opportunities for the development of low-cost and large-area (opto)electronics. Although (trialkylsilyl)ethynyl ($R_3Si–C\equiv C–$) has emerged as a very popular unit to solubilize organic semiconductors, it has been applied only to a limited class of materials that are mostly substituted on short molecular axes. Herein, two novel solution-processable indenofluorene-based semiconductors, **TIPS-IFDK** and **TIPS-IFDM**, bearing (triisopropylsilyl)ethynyl end units at 2,8-positions (*long molecular axis substitution*) were synthesized, and their single-crystal structures, optoelectronic properties, solution-sheared thin-film morphologies/microstructures, and n-channel field-effect responses were studied. In accordance with the DFT calculations, the HOMO/LUMO energies of the new compounds are found to be −5.77/−3.65 eV and −5.84/−4.18 eV for **TIPS-IFDK** and **TIPS-IFDM**, respectively, reflecting the high electron deficiency of the new π-backbones. Both semiconductors exhibit slightly S-shaped molecular frameworks with highly coplanar **IFDK/IFDM** π-cores, and they form slipped π-stacked one-dimensional (1-D) columnar motifs in the solid state. However, substantial differences in the degree of π–π interactions and stacking distances (4.04 Å *vs.* 3.47 Å) were observed between **TIPS-IFDK** and **TIPS-IFDM** as a result of carbonyl *vs.* dicyanovinylene functionalization, which results in a three orders of magnitude variation in the charge carrier mobility of the corresponding thin films. Top-contact/bottom-gate OFETs fabricated *via* solution-shearing **TIPS-IFDM** yielded one of the best performances in the (trialkylsilyl)ethynyl literature ($\mu_e = 0.02$ cm^2 V^{-1} s^{-1}, $I_{on}/I_{off} = 10^7$–10^8, and $V_T \sim 2$ V under ambient atmosphere) for a 1-D polycrystalline semiconductor microstructure. To the best of our knowledge, the molecules presented here are the first examples of n-type semiconductors substituted with (trialkylsilyl)ethynyl groups on their long molecular axes.
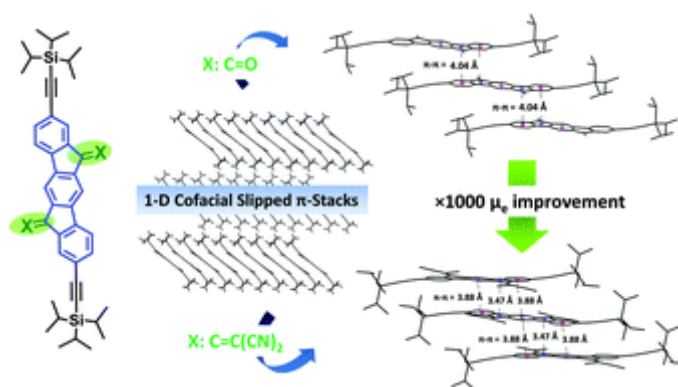
Introduction

Solution-processable polycyclic aromatic hydrocarbons (PAHs) with good electron-accepting and transporting properties are very attractive semiconducting materials for n-channel organic field-effect transistors (OFETs), complementary circuits, and photovoltaics.[1–5] While solution processability is key to roll-to-roll fabrication of low-cost, flexible, and large area devices, the structural versatility of the π-systems allows for the realization of fine-tuned (opto)electronic properties.[6–11] The functionalization of PAHs to impart solubility in common organic solvents and to induce electron-accepting/transporting properties could be achieved *via* exploratory synthesis, which has been widely exploited for the development of novel small/macro-molecular structures with unprecedented properties.[12–15] The rational incorporation of strongly electron-withdrawing

substituents such as –CN, –F, and $-C_nF_{2n+1}$ has been particularly important for reducing frontier orbital energy levels of PAHs and facilitating electron-transport processes in (opto)electronics.[16,17] For solution-processable PAH semiconductors, it is very critical to select a properly sized π-skeleton to reach a delicate balance between solubility and effective charge carrier π-delocalization. To this end, the relatively small-sized indenofluorene (IF) has recently become an attractive π-core as a functionalizable coplanar, ladder-type PAH.[18–20] Although IF derivatives have been widely explored for over sixty years in various literature reports,[21] the potential of IF as a functional charge-transporting material has only recently been revealed.[22] In 2008, Usta, Facchetti, and Marks *et al.* pioneered early studies demonstrating that carbonyl (C=O) and dicyanovinylene (C=C(CN)$_2$) functionalizations on the five-membered rings of IF could lead to a novel class of high performance, ambient-stable n-channel semiconductors in OFETs.[23] These π-cores are named "indeno[1,2-*b*]fluorene-6,12-dione (IFDK)" and "2,2′-(indeno[1,2-*b*]fluorene-6,12-diylidene)dimalononitrile (IFDM)", and they exhibit highly stabilized lowest unoccupied molecular orbital (LUMO) energies (−3.5 eV to −4.2 eV), reversible reductions, photo/thermal stabilities, and solution processabilities. Later, following this original study, numerous IFDK and IFDM derivatives have been synthesized yielding electron mobilities as high as 1.0 cm^2 V^{-1} s^{-1}.[24] It is noteworthy that non-functionalized IF π-structures display exclusively p-channel characteristics due to the fact that their LUMOs are energetically too high (>−3.0 eV) and their highest occupied molecular orbitals (HOMOs) align well with air-stable conductive electrodes (*e.g.* Au: 5.1 eV).[22,25] Detailed studies of the library of IF-based semiconductors by fine-tuning frontier orbital energies have revealed the LUMO threshold value (−4.0 to −4.1 eV) for ambient-stability of electron transport.[25] Considering that there are still very few solution-processable and low-LUMO n-type semiconductors in the literature, the continued design and synthesis of novel molecular architectures is important. In particular, small molecules that could be synthesized in a few steps are very valuable for the future technological implementation of these materials in low-cost optoelectronics. On the other hand, maintaining a large HOMO–LUMO energy gap while stabilizing the LUMO energy level is crucial for (opto)electronic devices to prevent undesired hole injection/transport characteristics through HOMOs.

Herein, in contrast to earlier reports on solution-processed electron-transporting IFs, in which alkyl groups or β-/α,ω-alkyl substituted donor-units are placed at molecular termini, we envision to completely remove donor end-units and long linear/swallow-tailed lipophilic alkyl substituents. Instead, the present novel molecules **TIPS-IFDK** and **TIPS-IFDM** are designed with shape-persistent, rod-like (triisopropylsilyl)ethynyl (((CH$_3$)$_2$CH)$_3$Si–C≡C–) groups (Fig. 1). The presence of trialkylsilyl groups significantly enhances the solubility of insoluble PAHs and increases their photochemical/ambient stability, which has opened new avenues for the realization of solution-processed (opto)electronic devices.[18,29–33] In addition, the nature of the alkyl substituents in (trialkylsilyl)ethynyl groups has been found to drastically alter the semiconductor solid-state packing motifs and thus the corresponding charge-carrier mobilities in OFETs. Following this strategy, numerous solution-processable molecular semiconductors, most of which comprise formerly insoluble acene π-frameworks, have been prepared and characterized in OFETs over the past decade.[34,35] It is noteworthy that silicon is one of the few elements that has a lower electronegativity than carbon and could still form a strong covalent bond with carbon. This imparts a great electron density, and thus polarizability, to the short alkyl chains of trialkylsilyl (–SiR$_3$) substituents, which allows for the formation of strong attractive London-dispersion forces with common organic solvents. Alkyne linkages are employed between sterically bulky triisopropyl substituents and the central IF cores as a spacer to result in π-stacked (*vide infra*) shape-persistent, rod-like structures with practically no conformer formation. Due to its quasi-cylindrical electronic symmetry, alkyne linkages are key to accommodate steric/conformational constraints, and the presence of sp-hybridized carbons should stabilize frontier orbital energies of the new molecules to assist in its electron-accepting properties. In the current molecules, π-frameworks are synthesized with

((CH$_3$)$_2$CH)$_3$Si–C≡C– groups along the long molecular axis, which is very different from the case of most of the previously reported semiconductors that are typically substituted with R$_3$Si–C≡C– groups along the short molecular axis. To the best of our knowledge, this is the first time that a molecular semiconductor substituted with (trialkylsilyl)ethynyl groups along the long molecular axis is characterized in OFETs. Note that although there are a few recent studies reporting pentacene derivatives substituted with (trialkylsilyl)ethynyl groups at 2,9/3,10-positions (*long molecular axis*), these studies did not demonstrate any OFET device application.[36–38] Therefore, the present molecules would constitute a valuable structural platform to understand whether (trialkylsilyl)ethynyl functionalization along the long molecular axis is a practical strategy to realize π-stacked solid-state packing and solution-processed OFETs with good electron mobilities.

β-DD-TIFDKT: n = 0, X = O, R$_1$ = C$_{12}$H$_{25}$, R$_2$ = H
β-DD-TIFDMT: n = 0, X = C(CN)$_2$, R$_1$ = -C$_{12}$H$_{25}$, R$_2$ = H
2OD-TIFDKT: n = 0, X = O, R$_1$ = H, R$_2$ = -CH$_2$CH(C$_8$H$_{17}$)C$_{10}$H$_{21}$
2OD-TIFDMT: n = 0, X = C(CN)$_2$, R$_1$ = H, R$_2$ = -CH$_2$CH(C$_8$H$_{17}$)C$_{10}$H$_{21}$
2OD-TTIFDMT: n = 1, X = C(CN)$_2$, R$_1$ = H, R$_2$ = -CH$_2$CH(C$_8$H$_{17}$)C$_{10}$H$_{21}$

TIPS-IFDK: X = O
TIPS-IFDM: X = C(CN)$_2$
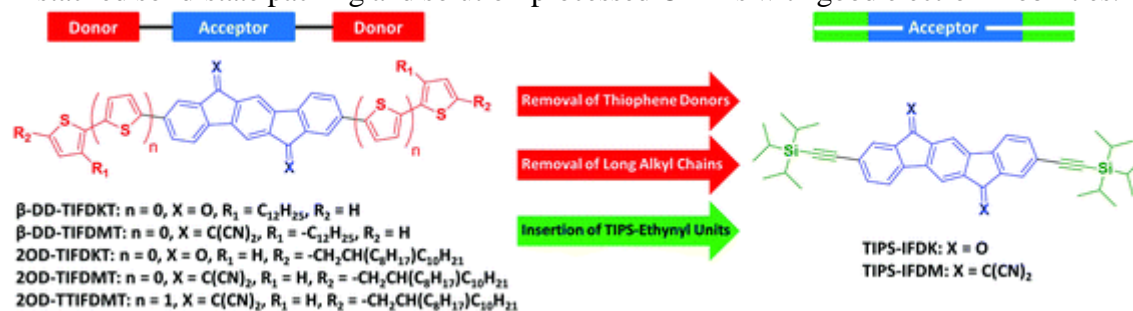
Fig. 1 The chemical structures of the newly designed **TIPS-IFDK** and **TIPS-IFDM** compounds as compared to previously reported representative electron-transporting indenofluorene derivatives.[25–28]

We report herein the synthesis, single-crystal structures, optoelectronic properties, solution-processed thin-film morphologies/microstructures, and n-channel field-effect responses of two novel solution-processable molecular semiconductors, **TIPS-IFDK** and **TIPS-IFDM** (Fig. 1). These structures are designed bearing (triisopropylsilyl)ethynyl end units at 2,8-positions of highly electron-deficient, ladder-type **IFDK** and **IFDM** π-cores. As a result of having fully acceptor type π-backbones, when compared with previously developed donor–acceptor type IFs, both HOMO/LUMO energies of the new compounds (−5.77/−3.65 eV for **TIPS-IFDK** and −5.84/−4.18 eV for **TIPS-IFDM**) were found to be lower, resulting in slightly increased optical band gaps (2.12 eV for **TIPS-IFDK** and 1.66 eV for **TIPS-IFDM**). DFT calculations revealed the electronic effects of (triisopropylsilyl)ethynyl substitutions on frontier molecular orbitals. Single-crystal X-ray diffraction (XRD) analysis revealed highly coplanar structures for the central **IFDK/IFDM** cores and slightly S-shaped molecular frameworks. Although both semiconductors exhibit very similar slipped π-stacked one dimensional (1-D) columnar motifs in the solid state, **TIPS-IFDM** molecules showed a significant degree of π–π stackings with short distances of 3.47 Å, while **TIPS-IFDK** showed more limited π–π interactions. This reveals that although the general solid-state packing motif is governed by the full molecular framework, specific interactions between adjacent molecules is controlled by functional groups (carbonyl *vs.* dicyanovinylene). Top-contact/bottom-gate OFETs fabricated *via* solution-shearing **TIPS-IFDM** has yielded n-channel devices with an ambient-stable electron mobility of 0.02 cm^2 V^{-1} s^{-1}, an I_{on}/I_{off} of 10^7–10^8, and a V_T of ~2 V. To the best of our knowledge, this is the first example of a solution-processable, ambient-stable n-type molecular semiconductor functionalized with (trialkylsilyl)ethynyl groups along the long molecular axis. Detailed microstructural and morphological analysis of the corresponding semiconductor films shows that **TIPS-IFDM** molecules are oriented on the surface having the (002) crystal plane parallel to the substrate surface, which allows the formation of in-plane π–π stacks. As a result of less effective π–π interactions and the poor crystallinity in the thin-film phase, **TIPS-IFDK** showed three orders of magnitude lower electron mobility. Our results clearly show that subtle changes in molecular structures *via* functionalization could lead to crucial alterations in the corresponding solid-state packing and the charge-transport characteristics. Dicyanovinylene functionalization is found to

result in very efficient π–π stackings in (trialkylsilyl)ethynyl-substituted IFs yielding one of the highest electron mobilities in the literature for a 1-D polycrystalline semiconductor microstructure.

Results and discussion

Synthesis, single-crystal structures and thermal characterization studies

The synthesis of **TIPS-IFDK** and **TIPS-IFDM** small molecules is shown in Scheme 1, which involves a high-temperature Sonogashira cross-coupling reaction as the key step to introduce (triisopropylsilyl)ethynyl units. The experimental conditions employed for the synthesis of the intermediate indenofluorene compound **IFDK-Br$_2$** was the same as those previously reported by us (Scheme S1†).[26–28] In the presence of a CuI/Pd(PPh$_3$)$_2$Cl$_2$ cocatalyst/catalyst system and an Et$_3$N base, (triisopropylsilyl)ethynyl groups were added at 2,8-positions of indeno[1,2-*b*]fluorene-6,12-dione by reacting **IFDK-Br$_2$** with (triisopropylsilyl)acetylene. **TIPS-IFDK** was obtained in 64% yield. The Sonogashira cross-coupling reaction of **IFDK-Br$_2$** yielded only an indeno[1,2-*b*]fluorene-6,12-dione-based **TIPS-IFDK** fraction in the column chromatography; no by-product having the indeno[2,1-*a*]fluorene-11,12-dione (Fig. S1†) isomer was isolated. This indicates a very high selectivity in the second intramolecular acylation step of **IFDK-Br$_2$** synthesis. A primitive mechanistic analysis of this reaction demonstrates that there is no resonance stabilization effect between -*ortho* and -*para* acylations (Fig. S1†). Therefore, considering that the reaction was carried out at high temperature, thermodynamic effects were present and it is very likely that the difference in the energetics of formation of the transition state and/or the product between two isomers was the key factor.[39,40] This is very consistent with previous reports of indeno[2,1-*a*]fluorene-11,12-dione derivatives in the literature that they were all prepared from 1,2-benzene-diacid/diester precursors that synthetically allow the formation of only indeno[2,1-*a*]fluorene-11,12-dione isomer.[41,42] The current unique molecular design allows us to maintain the electron-withdrawing carbonyl/dicyanovinylene functionalities in the final small molecules with no σ-insulating alkyl substituents nearby. Considering that most of the previous studies on (trialkylsilyl)ethynyl-substituted semiconductors have focused on π-extensions on the short molecular axis (Fig. S2†),[18,43–49] the current design helps us to understand whether (trialkylsilyl)ethynyl functionalization on long molecular axes could also yield effective solid-state packing. The subsequent Knoevenagel condensation of **TIPS-IFDK** to form dicyanovinylene-substituted **TIPS-IFDM** was achieved in 84% yield using excess malononitrile with a pyridine base and TiCl$_4$ Lewis acid. In contrast to the poor solubility of the parent compound **IFDK-Br$_2$**, new small molecules **TIPS-IFDK** and **TIPS-IFDM** were found to be freely soluble in common organic solvents (CHCl$_3$, CH$_2$Cl$_2$, THF, and toluene). They were conveniently purified by silica gel column chromatography. The purities and structures of the intermediate compounds and the final small molecules were characterized by ^{1}H/^{13}C NMR (Fig. S3, S4, S6, and S7, ESI†), elemental analysis, mass spectroscopy (MALDI-TOF) (Fig. S5 and S8, ESI†), ATR-FTIR (Fig. S9, ESI†), and melting point measurements. In order to perform a comparative optoelectronic study, **β-DD-TIFDKT** and **β-DD-TIFDMT** reference compounds were synthesized in accordance with our previously reported procedure.[23]
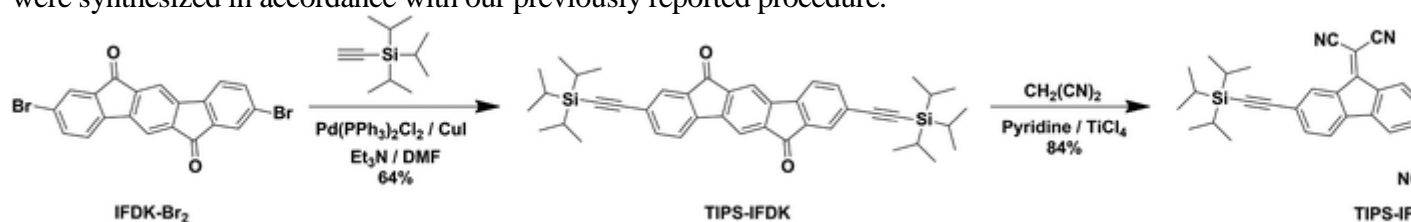
Scheme 1 Synthetic routes to **TIPS-IFDK** and **TIPS-IFDM**.

As shown in Fig. 2, both small molecules were found to be thermally very stable with thermolysis onset temperatures (5% weight loss) of 400 °C (for **TIPS-IFDM**) and 420 °C (for **TIPS-IFDK**). Two-step decomposition profiles were observed for both small molecules with small steps at ~90–92% of the original weights, which correspond to the initial mass losses of multiple methyl ($-CH_3$) and/or isopropyl ($-CH(CH_3)_2$) substituent(s). Based on differential scanning calorimetry measurements in the second heating–cooling cycles, **TIPS-IFDM** showed two endothermic peaks at 280 °C (enthalpy = 3.55 J g^{-1}) and 315 °C (enthalpy = 22.09 J g^{-1}). The thermal transition at 315 °C was later confirmed by conventional melting-temperature measurements to agree with the melting point of **TIPS-IFDM** (T_{mp} = 316–317 °C). The low-enthalpy thermal transition at 280 °C prior to the melting could be attributed to solid-to-liquid crystal transition, which is not unusual for rod-shaped π-conjugated molecules.[28,50,51] A corresponding exothermic crystallization peak was observed at 285 °C (enthalpy = 23.05 J g^{-1}) in the cooling cycle. The melting temperature of **TIPS-IFDM** is much higher (ΔT_{mp} = 70–80 °C) than those of previously reported alkyl-thienyl substituted IFDM derivatives with similar size, indicating the efficiency of this new design in promoting strong solid-state packing with a low density of flexible alkyl chains (*vide infra*).[23,26,28] Despite the presence of endothermic thermal transitions at 176 °C (enthalpy = 15.14 J g^{-1}) and 242 °C (enthalpy = 6.94 J g^{-1}) for **TIPS-IFDK** in the DSC profile, no observable melting (solid-to-isotropic liquid) process occurred before decomposition at >380 °C. Therefore, the observed thermal processes could be attributed to solid-to-solid or solid-to-liquid crystal transitions. Note that, as compared with previously developed alkyl thienyl-substituted IFDK derivatives, the absence of long and flexible alkyl substituents tunes the intermolecular interactions and results in complete disappearance of the melting process. And this is very comparable to the thermal behavior of the parent **IFDK-Br₂** compound, which is most likely a result of structurally close molecular frameworks and similar solid-state packing motifs (*vide infra*).
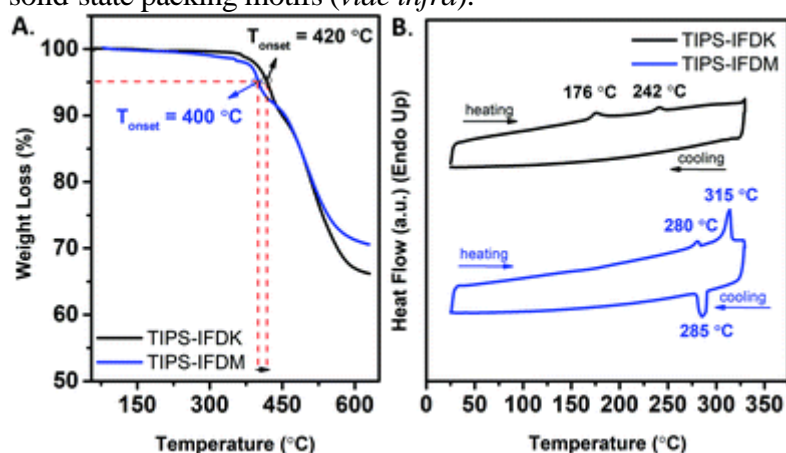
Fig. 2 Thermogravimetric analysis (TGA) curves (A) and differential scanning calorimetry (DSC) measurement curves (B) in the second heating–cooling cycles for **TIPS-IFDK** and **TIPS-IFDM** at a temperature ramp of 10 °C min⁻¹ under N_2.

In order to gain an insight into the solid-state structural features and intermolecular interactions, plate-like single crystals of both small molecules were grown by diffusion of hexane into their tetrahydrofuran (THF) solutions and characterized by single-crystal X-ray crystallography (Fig. 3 and 4). **TIPS-IFDK** and **TIPS-IFDM** crystallize in the triclinic space group $P\bar{1}$ and the monoclinic space group $C2/c$, respectively. In both compounds, indenofluorene adopts a substantially coplanar π-conjugated backbone with small plane-to-plane twist angles ($\theta < 2$–3°) between arene rings and lies across a crystallographic inversion center. While carbonyl/dicyanovinylene functionalities stay completely within the indenofluorene π-core planes, ethynyl units are slightly displaced ($\theta = 5$–7°) out of the planes, which is similar to the case of previously reported (triisopropylsilyl)ethynyl-substituted molecular π-scaffolds.[52,53] The π-core

planarity in **TIPS-IFDK** is consistent with the computational optimization results and similar to the IFDK derivatives previously reported.[18,24,26]However, IFDM π-core planarity in **TIPS-IFDM** is quite different from the "wavy" backbone structure of the previously reported 2,2′-(2,8-dibromo-5,11-didodecylindeno[1,2-*b*]fluorene-6,12-diylidene)dimalononitrile (Fig. S10†), which, to our knowledge, is the only known IFDM-based single-crystal structure in the literature.[25]According to Cambridge Structural Database version 5.39 (*Conquest*, updated on May 2018),[54] the **TIPS-IFDM**single-crystal structure obtained herein demonstrates the first example of a completely coplanar IFDM π-core in the literature. We believe that our current design approach would offer structural guidelines for developing future low-LUMO IFDM-based π-conjugated systems. As shown in Fig. 3C, short –CH···O=C– contacts (O1···H8 = 2.541 Å) between adjacent molecules of **TIPS-IFDK** are found to be effective (4 interactions per molecule) in the formation of highly planar π-layers along the crystallographic *a*-axis. These continuous π-layers are further expanded into the *b*- and *c*-axes by forming one-dimensional cofacial slipped π–π stacks with an interplanar distance of 4.04 Å (Fig. 3b). When dicyanovinylene (–C=(CN)$_2$) substituents are used instead of carbonyl groups, similar highly planar π-layers were formed along the crystallographic *b*-axis *via* strong –CH···N≡C– interactions (N2···H14 = 2.458 Å) (4 interactions per molecule). Note that a much larger decrease was observed in the corresponding van der Waals distance[55] for the –CH···N≡C– contact (10.62% shortened) when compared with –CH···O=C contact (6.62% shortened), which reflects the strength of dicyanovinylene substituents in forming closely packed solid-state motifs. As shown in Fig. 4D, the continuous π-layers of **TIPS-IFDM** are found to form one-dimensional cofacial slipped π–π stacks along the *a*- and *c*-axes, yet with much shorter interplanar distances of 3.47 Å and 3.88 Å between arene rings. Similar to our previously reported indenofluorene structures,[26] the presence of strong local dipoles of carbonyl (–C=O)/dicyanovinylene (–C=C(CN)$_2$) groups can overcome the formation of edge-to-face interactions (C–H···π/herringbone packing) and result in cofacial slipped π-stacked arrangements. Although both semiconductors exhibit very similar 1-D columnar arrangements in the solid state, **TIPS-IFDM** molecules showed much improved π–π interactions. This indicates that even though the general solid-state ordering motif is governed by the full molecular framework, the degree of specific interactions between individual molecules is dictated by functional groups. Improved π–π interactions between **TIPS-IFDM** molecules in the solid-state as a result of switching from carbonyl to dicyanovinylene leads to three orders of magnitude higher charge-carrier mobility (*vide infra*).
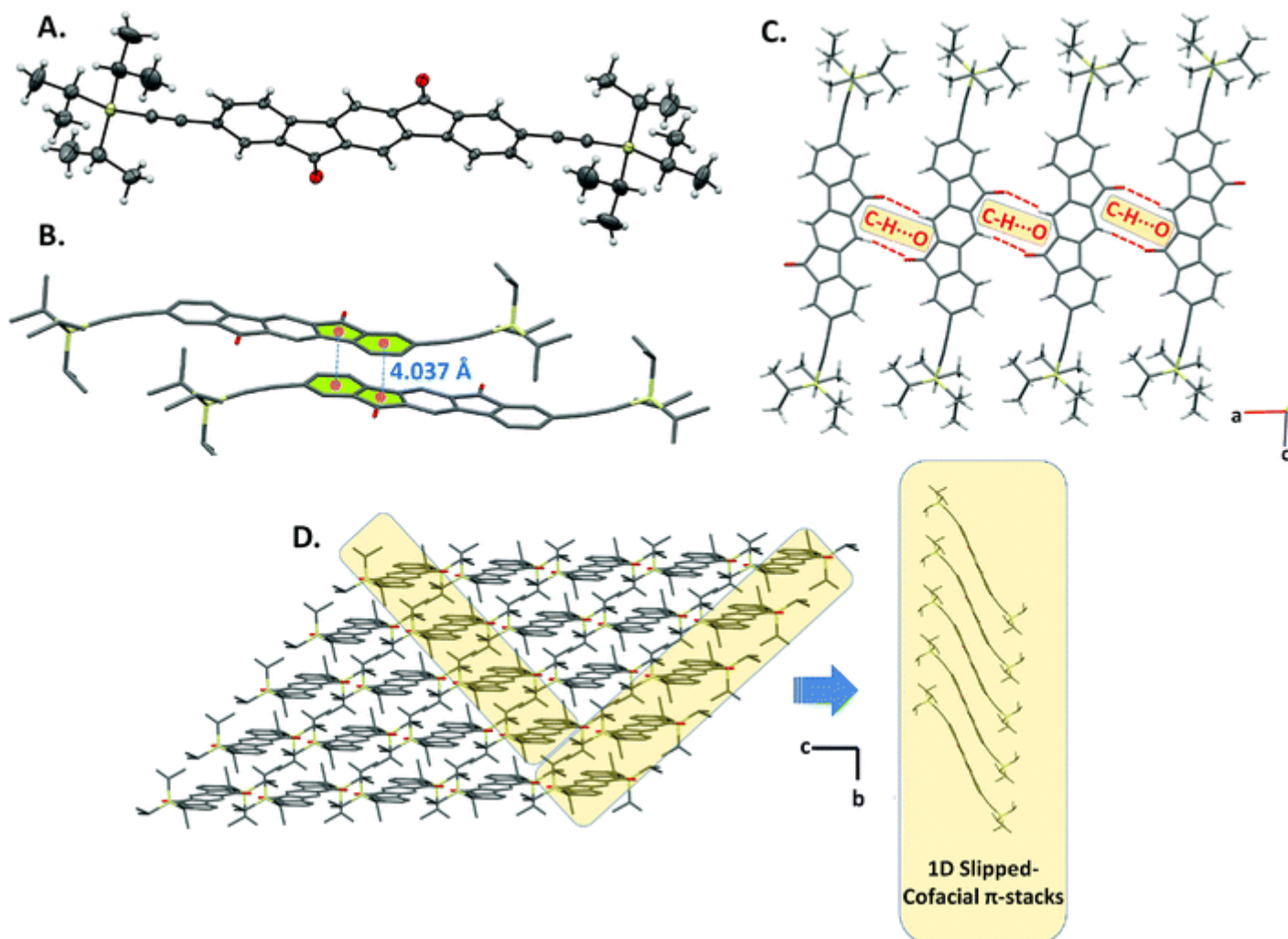
Fig. 3 ORTEP drawings of the crystal structure of **TIPS-IFDK** (30% probability level) (A), representations of pairs of indeno[1,2-*b*]fluorene-6,12-dione (**IFDK**) molecules arranged in a slipped π-stacked fashion with a centroid-to-centroid distance of 4.037 Å (B), the continuous π-layer formation *via* short CH⋯O contacts (C), perspective views of the molecular arrangement and one-dimensional cofacial slipped π-stacks (D).
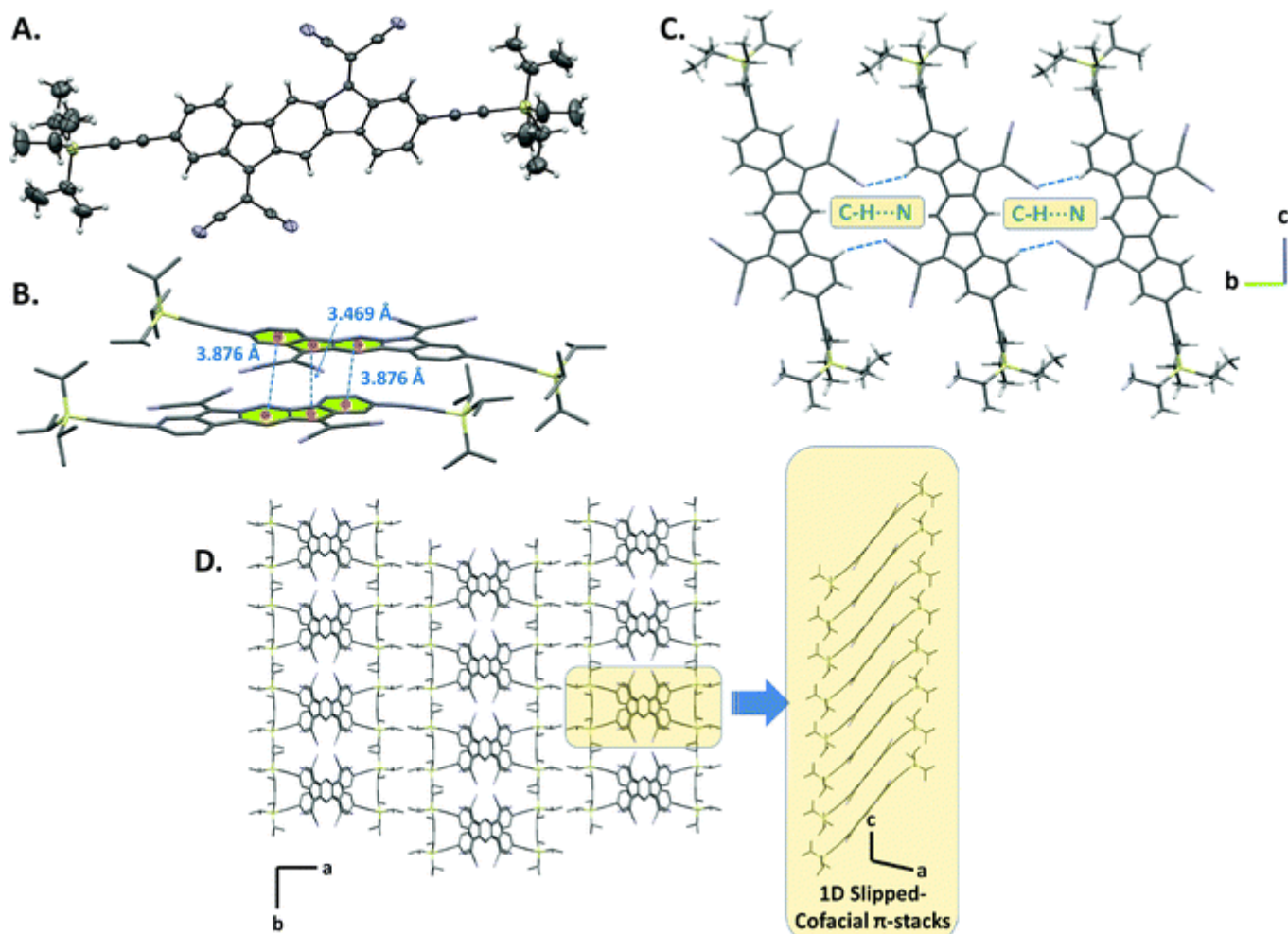
Fig. 4 ORTEP drawings of the crystal structure of **TIPS-IFDM** (30% probability level) (A), representations of pairs of (indeno[1,2-*b*]fluorene-6,12-diylidene)dimalononitrile (**IFDM**) molecules arranged in a slipped π-stacked fashion with favorable π⋯π distances of 3.469/3.876 Å (B), the continuous π-layer formation *via* short CH⋯N contacts (C), perspective views of the molecular arrangement and one-dimensional cofacial slipped π-stacks (D).

Optical and electrochemical properties

Density functional theory calculations for **TIPS-IFDK** and **TIPS-IFDM**, along with the previously developed reference semiconductors **β-DD-TIFDKT(M)** (Fig. 1), were performed using the B3LYP method and the 6-31G** basis set. The calculations reveal that the present (triisopropylsilyl)ethynyl functionalization decreases both HOMO and LUMO energies relative to the β-substituted donor–acceptor–donor compounds (Fig. 5D). Analysis of the orbital spatial distributions shows that while there is significant HOMO wave-function density on ethynyl units, LUMOs are delocalized only in the central indenofluorene π-units. Thus, the LUMO stabilizations are attributed to the negative (−I) inductive effect of sp-hybridized ethynyl end units as compared with the relatively electron-rich thienyl units. This also explains why the energetic stabilizations of HOMOs (ΔE = 0.15–0.19 eV) are larger than those of LUMOs (0.04–0.1), resulting in increased HOMO–LUMO gaps (ΔE = 0.1–0.2 eV). The increased band gaps also reflect the effect of changing the donor–acceptor–acceptor π-architecture to a fully π-acceptor architecture. Note that solution-processable small molecules with low LUMO/HOMO levels are very attractive materials for use as non-fullerene acceptors in bulk-heterojunction photovoltaics (BHJ-OPVs), since, when combined

with donor materials, they yield efficient exciton dissociation *via* only electron transfer without any undesired hole transfer.
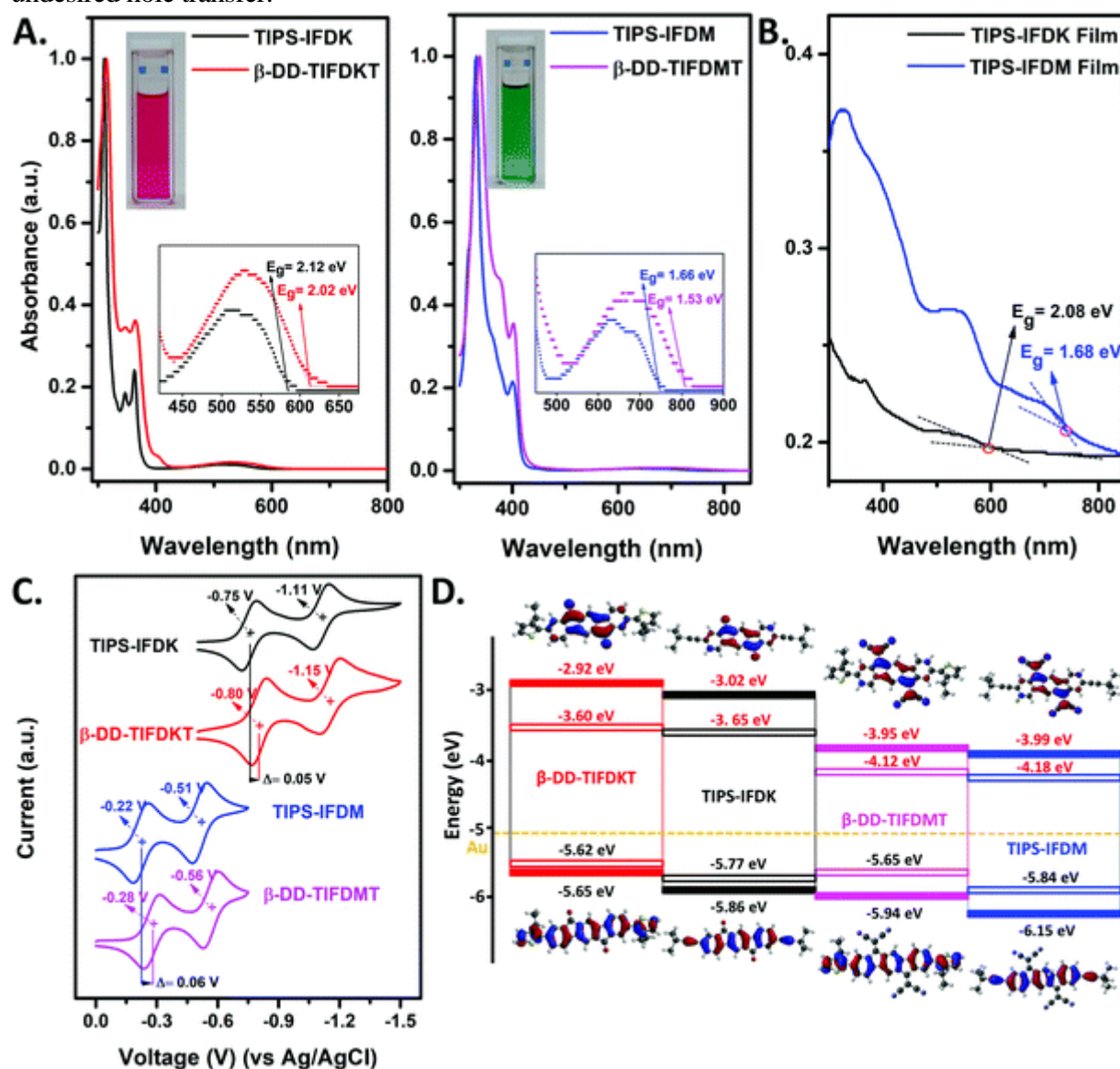
Fig. 5 For **TIPS-IFDK** and **TIPS-IFDM** and the reference molecules **β-DD-TIFDKT** and **β-DD-TIFDMT**, optical absorption in dichloromethane solution (insets are the images of the corresponding TIPS-IFDK(M) solutions) (A), optical absorption in thin films (B), cyclic voltammograms in dichloromethane (0.1 M $Bu_4N^+PF_6^-$, scan rate = 50 mV s^{-1}) (C), and calculated (solid blocks; DFT/B3LYP/6-31G**) and experimental (hollow blocks) HOMO and LUMO energy levels with topographical orbital representations (D).

The UV-vis absorption spectra of the present compounds **TIPS-IFDK** and **TIPS-IFDM** were recorded in dichloromethane solutions and in spin-coated thin films (Fig. 5A and B, and Table 1). At short wavelengths (<400 nm) both compounds exhibit well-defined peaks with intense absorptions corresponding to the π–π* transition of the diethynyl-substituted indeno[1,2-*b*]fluorene π-core. The low-intensity peaks at 514 nm (for **TIPS-IFDK**) and 625 nm (for **TIPS-IFDM**) are attributed to symmetry forbidden n–π* transitions as a result of the presence of carbonyl/dicyanovinylene functional groups. Despite negligible changes at high-energy absorption peaks (<400 nm), the effect of carbonyl *vs.* dicyanovinylene substitution is evident in the low-energy absorption peaks where a significant bathochromic shift of ∼111 nm was observed when going from carbonyl to dicyanovinylene on the methylene bridges. This is apparently the result of LUMO

energetic stabilization (*vide infra*) due to the stronger electron-withdrawing ability of dicyanovinylene and further extended delocalization of LUMO wavefunction on dicyanovinylene units (Fig. 5D). The optical band gaps estimated from the low-energy absorption edge onsets are 2.12 eV for **TIPS-IFDK** and 1.66 eV for **TIPS-IFDM**, respectively. Consistent with DFT calculations, both compounds showed hypsochromically shifted low-energy peaks ($\Delta\lambda = 16$–56 nm) and increased optical band gaps when compared with their β-substituted counterparts ($E_{g(\beta\text{-DD-TIFDKT})} = 2.02$ eV and $E_{g(\beta\text{-DD-TIFDKT})} = 1.53$ eV) (Fig. 5A). When going from solutions to spin-coated thin films, both compounds exhibit minimal changes in the low-energy absorption onsets. This is very different from the case of previously reported alkylthienyl-substituted D–A–D type IF derivatives, which typically showed reduced band gaps as a result of molecular backbone planarization in the solid state.[25] The absence of the same kind of backbone planarization in the present molecules due to the nature of the current π-frameworks explains the minimal changes in their optical band gaps.

Table 1 Summary of the optical absorption/electrochemical properties and the corresponding estimated frontier molecular orbital energies of **TIPS-IFDK** and **TIPS-IFDM** and the reference molecules **β-DD-TIFDKT** and **β-DD-TIFDMT**

Compound	$\lambda^{sol.}_{abs}$ [a] (nm)	$E^{sol.}_{g}$ [b] (eV)	λ^{film}_{abs} [c] (nm)	E^{film}_{g} [b] (eV)	$E^{red.}_{1/2}$ [d] (V)	E_{LUMO} [e] (eV)	E_{HOMO} [f] (eV)
TIPS-IFDK	312, 363, 514	2.12	369, 532	2.08	−0.75	−3.65	−5.77
β-DD-TIFDKT	315, 365, 530	2.02	365, 594[g]	1.89[g]	−0.80	−3.60	−5.62
TIPS-IFDM	329, 400, 625	1.66	329, 538, 693	1.68	−0.22	−4.18	−5.84
β-DD-TIFDMT	338, 401, 681	1.53	412, 759[g]	1.50[g]	−0.28	−4.12	−5.65

a From the optical absorption measured in dichloromethane. b The optical band gap is estimated from the low-energy band edge of the corresponding UV-vis absorption spectrum. c From optical absorption measured in spin-coated thin films on glass. d Recorded in a 0.1 M Bu$_4$N$^+$PF$_6^-$ solution in CH$_2$Cl$_2$ at a scan rate of 50 mV s^{-1} using a Pt working electrode and an Ag/AgCl reference electrode. e Estimated from the equation: $E_{LUMO} = -4.40$ eV $- E^{red.}_{1/2}$. f Calculated from: $E_g = E_{LUMO} - E_{HOMO}$. g Thin-film absorption data are taken from ref. 25.

The electrochemical properties of the new compounds and reference molecules were investigated by the cyclic voltammetry technique under the exact same experimental conditions to study the small changes in the frontier orbital energetics. As shown in Fig. 5C, both compounds showed reversible reduction peaks with the first half-wave potential located at −0.75 V (*vs.* Ag/AgCl) for **TIPS-IFDK** and −0.22 V (*vs.* Ag/AgCl) for **TIPS-IFDM**, which indicates redox stable n-doping characteristics. No electrochemical oxidation peak was observed for both small molecules. Since the electron-accepting ability of dicyanovinylene is greater than carbonyl and the diethynyl-indenofluorene π-core remains the same, the reduction peaks exhibit significant anodic shifts (−0.75/−1.11 V → −0.22/−0.51 V) when going from **TIPS-IFDK** to **TIPS-IFDM**. Additionally, when two small molecules with the same functionalities are compared, the half-wave-reduction potentials are found to be less negative for the new TIPS-substituted compounds relative to the reference compounds. This is obviously the result of the existence of electron-withdrawing ethynyl groups and the absence of electron-rich alkylthienyl units at 2,8-positions of the new molecules. The

HOMO/LUMO energy levels were estimated to be −5.77/−3.65 eV for **TIPS-IFDK** and −5.84/−4.18 eV for **TIPS-IFDM**, which are both lower than those of the reference **β-DD-TIFDKT** and **β-DD-TIFDMT** compounds. As shown in Fig. 5D, the energetic trends of the corresponding frontier molecular orbitals show great agreement between the DFT calculations and the experimental estimations. It is very encouraging for future materials design in IFs that even subtle changes measured in frontier molecular orbital energies could be predicted beforehand by density functional theory. Note that the LUMO energies of the new compounds are in the range of previously reported n-type semiconductors. Specifically, the LUMO energy level of **TIPS-IFDM** could enable air-stable n-channel conduction in OFETs.

Thin-film microstructure/morphology and field-effect transistor characterization

Charge-transport characteristics of the present semiconductors were studied in top-contact/bottom-gate (TC/BG) OFET devices. Thin films of **TIPS-IFDM** (50 nm) and **TIPS-IFDK** (55 nm) were prepared by solution shearing semiconductor solutions on PS (polystyrene)-brush coated n^{++}-Si/SiO$_2$ (300 nm) gate-dielectric substrates. This solution-processing method and the polymeric dielectric treatment were preferred to afford favorable semiconductor morphology/crystallization at the semiconductor–dielectric interface.[56–59] The microstructural and morphological properties of the semiconductor thin films were studied by out-of-plane θ–2θ X-ray diffraction (XRD) and atomic force microscopy (AFM). As shown in Fig. 6A, for thin films of **TIPS-IFDM**, multiple sharp diffraction peaks of the same phase were observed, indicating a highly crystalline semiconductor film with a high degree of solid-state ordering. The major diffraction peak was observed at $2\theta =$ 4.67° along with its higher degree peaks at $2\theta =$ 9.30°, 13.92°, and 18.58°. Using the single-crystal unit cell parameters, simulation of the observed diffraction pattern showed that molecules are oriented on the substrate having the (200) crystal plane parallel to the surface (Fig. 7B). This indicates the formation of a "layer-by-layer" packing motif that consists of alternately packed semiconducting π-backbones and insulating trialkylsilyl substituents in the out-of-plane direction. In the semiconducting part, slipped π-stacked molecules are aligned along the charge-transport direction (*in-plane*) with their π-cores tilted from the substrate normal ($\theta_{tilting} \sim 45°$). This arrangement is undoubtedly the result of having trialkylsilyl end-units, which prefer to interact with the substrate surface and drive the molecular π-backbones to adopt edge-on orientations.[47,60] Each **TIPS-IFDM** molecule shows close π–π interactions with the neighboring two molecules involving its full IF π-system, which results in short π–π contacts of 3.47 Å between five-membered rings and 3.88 Å between six-membered rings. On the other hand, thin films of **TIPS-IFDK** exhibit a low-intensity diffraction peak at $2\theta =$ 5.09° along with its higher order peak at $2\theta =$ 15.09°, which indicates a very limited crystallinity as compared to those of **TIPS-IFDM** (Fig. 6A). The simulation of the observed diffraction pattern according to the single-crystal unit cell parameters showed that **TIPS-IFDK** molecules are oriented on the substrate having the (001) crystal plane parallel to the surface (Fig. 7A). This also indicates a "layer-by-layer" packing motif having 1-D slipped π–π stacked molecules in the charge-transport direction. However, **TIPS-IFDK** molecules show increased tilting from the substrate normal ($\theta_{tilting} \sim 60°$) and more limited π–π interactions involving only part of the IF π-system, which results in longer π–π contacts of 4.04 Å between five- and six-membered rings. Therefore, when two π-systems are compared in the present semiconductors, **IFDM** clearly shows more effective π–π stacking interactions with nearby molecules, resulting in higher crystallinity and a densely packed π-system in the charge-transport direction. Considering that the present semiconductor molecules share the exact same π-framework with the only difference of the functional group, this undoubtedly reflects the effect of dicyanovinylene *vs.* carbonyl functionalization. As shown in Fig. 6B, AFM characterization studies of the present semiconductor thin films showed the formation of micrometer-sized ribbon-like domains aligned along the shearing directions. The surface of these ribbons appears to be very smooth over micrometer-sized areas,

indicating highly favorable two-dimensional molecular coverage on the surface during the solution-shearing process. On the basis of the step-height profile, a *layer-by-layer* semiconductor film growth mechanism was evident for **TIPS-IFDM** ribbons since step heights of ~2.2–2.3 nm match well with the dimensions of the molecular layers. In order to further elucidate the correlation between the observed microstructures and morphologies, the BFDH (Bravais, Friedel, Donnay and Harker) theoretical crystal morphologies for **TIPS-IFDK** and **TIPS-IFDM** were simulated, which predicted high aspect ratio crystal growth along the observed (001) and (200) crystal planes, respectively (Fig. S11†).
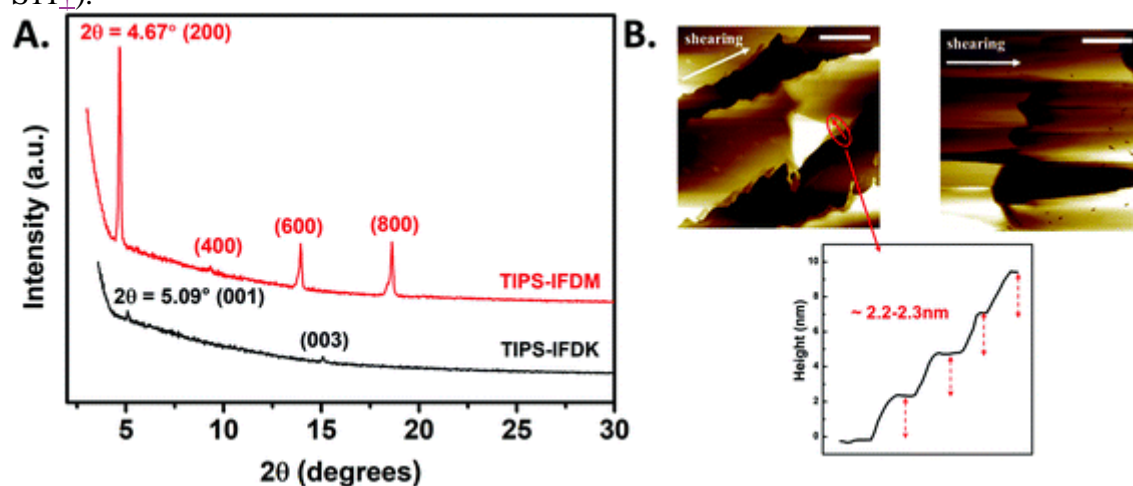
Fig. 6 θ–2θ X-ray diffraction (XRD) scans (A) and AFM topographic images (B) of the solution-sheared **TIPS-IFDK** (right) and **TIPS-IFDM** (left) thin films showing the indexed diffraction peaks based on single-crystal unit cell parameters. Scale bars denote 5 μm. The white arrow shows the shearing direction and the red arrow shows the direction of the step-height profile.
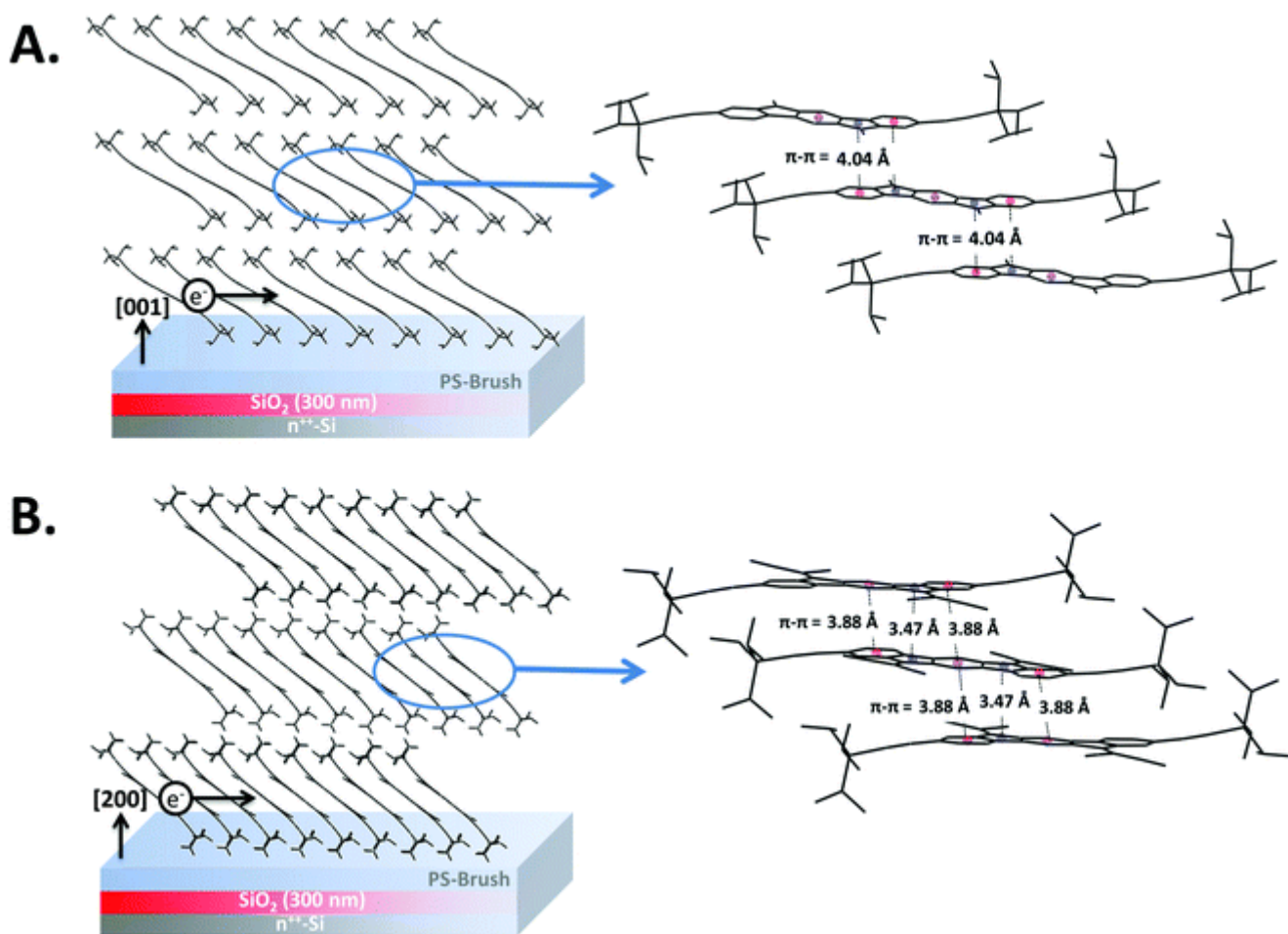
Fig. 7 The molecular arrangements in the out-of-plane [001] and [200] directions in **TIPS-IFDK** (A) and **TIPS-IFDM** (B) thin films showing intermolecular π–π interactions and stacking distances between neighboring molecules in the charge-transport direction.

Au source–drain electrodes were deposited on solution-sheared TIPS-IFDK(M)/PS(polystyrene)-brush/SiO$_2$(300 nm)/n^{++}-Si substrates by physical vapor deposition under vacuum (1×10^{-6} Torr). Consistent with the theoretical/experimental optoelectronic properties (*vide supra*), the devices exhibited n-channel charge-transport characteristics. Typical transfer and output plots are shown in [Fig. 8] and S12.†**TIPS-IFDM**-based OFET devices showed electron mobility as high as 0.02 cm^2 V^{-1} s^{-1} with an impressive I_{on}/I_{off} ratio of 10^7–10^8 and a threshold voltage of ~2 V under ambient atmosphere. These OFETs showed insignificant variations in transistor characteristics after three months storage under ambient atmosphere without exclusion of humidity and light (Fig. S13†). To the best of our knowledge, this molecule is the first example of a solution-processable, ambient-stable n-type molecular semiconductor functionalized with (trialkylsilyl)ethynyl groups along the long molecular axis. In contrast to previous reports in the (trialkylsilyl)ethynyl literature showing that 1-D slipped π-stacks lead to low mobilities ($<10^{-3}$–10^{-4} cm^2 V^{-1} s^{-1}), here we demonstrate an appreciable mobility thanks to the presence of strong π–π interactions.[53] However, when the π–π interactions along these channels become less effective as in **TIPS-IFDK**-based films (*vide supra*), the overall solution-processed film crystallinity is lowered and charge-transport performance significantly drops, resulting in three orders of magnitude lower electron mobility ($\mu_e = 4 \times 10^{-5}$ cm^2 V^{-1} s^{-1}, $I_{on}/I_{off} = 10^3$–10^4, $V_T \sim 30$ V) in the corresponding OFETs. While the highly stabilized LUMO energy level (−4.18 eV) of **TIPS-IFDM** allows for ambient stable electron-transport, **TIPS-IFDK**-based OFETs showed device activity only under vacuum as a result of its relatively high-energy LUMO (−3.65 eV). It is noteworthy that the p-channel semiconductivity

previously observed with the thienyl-substituted IFDK-based semiconductor, **β-DD-TIFDKT**, is completely missing in **TIPS-IFDK**. This could be ascribed to the absence of thienyl donor units in the new acceptor-type molecule and the further stabilized HOMO energy level (−5.77 eV *vs.* −5.62 eV). Our results clearly show that dicyanovinylene functionalization in IFs yields efficient π–π stackings, and the **IFDM** π-core is a proper-sized, favorable acceptor unit for building (trialkylsilyl)ethynyl-substituted solution-processable, ambient-stable n-type semiconductors. We envision that further structural optimizations on –R substituents and R_3Si–C≡C– substitution positions in IF π-systems could yield two-dimensional packing motifs in the solid-state and further improve charge carrier mobilities.
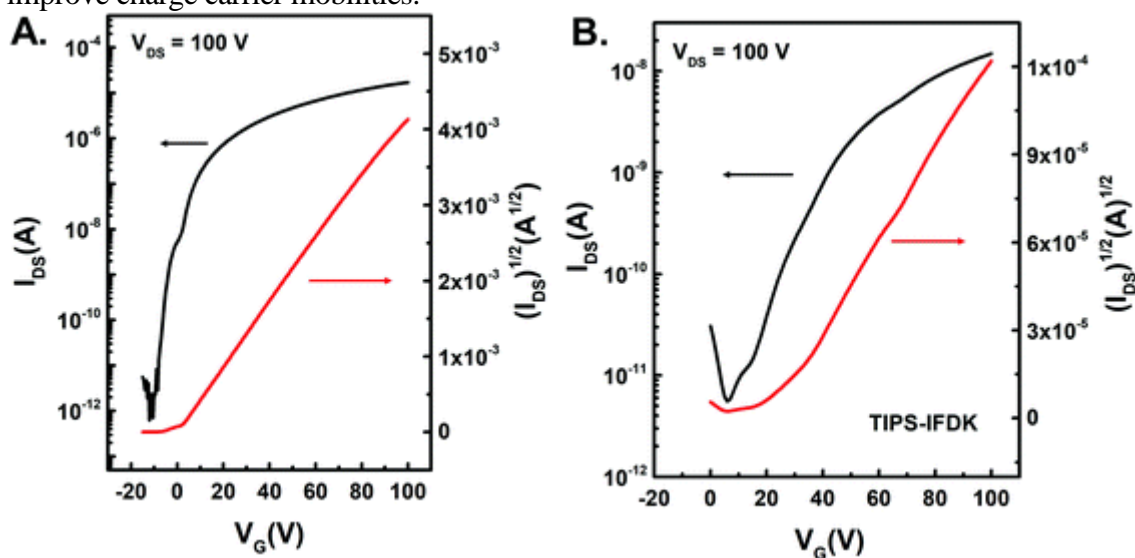
Fig. 8 Representative transfer curves in the n-channel region for Au/semiconductor/PS(polystyrene)-brush/SiO_2(300 nm)/n^{++}-Si top-contact/bottom-gate (TC-BG) OFET devices fabricated with solution-sheared **TIPS-IFDM** (A) and **TIPS-IFDK** (B) semiconductor thin films.

Conclusions

In summary, we have reported here the rational design, synthesis, single-crystal structures, optoelectronic properties, solution-sheared thin-film morphologies/microstructures, and n-channel field-effect responses of two novel solution-processable IF-based semiconductors, **TIPS-IFDK** and **TIPS-IFDM**, bearing (triisopropylsilyl)ethynyl end units. To the best of our knowledge, the molecules presented here are the first examples of n-type semiconductors substituted with (trialkylsilyl)ethynyl groups on their long molecular axes. The semiconductors exhibit stabilized HOMO/LUMO energies of −5.77/−3.65 eV (for **TIPS-IFDK**) and −5.84/−4.18 eV (for **TIPS-IFDK**), which agrees well with the DFT calculations and reflects the high electron-deficiency of the new π-backbones. X-ray analysis revealed slightly S-shaped π-scaffolds with highly coplanar IF cores and slipped π-stacked one-dimensional (1-D) columnar motifs in the solid-state for both semiconductors. Carbonyl *vs.* dicyanovinylene functionalization leads to substantial differences in the degree of π–π interactions and stacking distances (4.04 Å (**TIPS-IFDK**) *vs.* 3.47 Å (**TIPS-IFDM**)), and results in significant variations (×1000) in the corresponding electron mobilities. Dicyanovinylene functionalization is found to yield very efficient π–π stackings in (trialkylsilyl)ethynyl-substituted IFs resulting in one of the best OFET performances ($\mu_e = 0.02$ $cm^2V^{-1}s^{-1}$, $I_{on}/I_{off} = 10^7$–10^8, and $V_T \sim 2$ V under ambient atmosphere) in the literature for a 1-D polycrystalline semiconductor microstructure. The findings presented here demonstrate that (trialkylsilyl)ethynyl substitution on a functionalized IF π-system is a viable approach to realize new families of solution-processable n-type semiconductors, and electron-withdrawing functional groups

play a very critical role in determining crystal packing and electron transport characteristics. Further rational design guided by computational modeling could potentially lead to two-dimensional packing motifs and further improve charge carrier mobilities.

Experimental

Materials and methods

Unless otherwise noted, all reagents were purchased from commercial suppliers and used as received. All non-aqueous reactions were carried out in dried glassware under an inert atmosphere of N_2. Column chromatography was carried out with 230–400 mesh silica gel under the effect of gravitational force with or without additional air-pressure. Thin-layer chromatography (TLC) studies to monitor the reaction progress and chromatographic fractions were performed on alumina sheets covered with silica gel 60 F254. The melting points were determined using an Electrothermal IA9000 series digital melting point apparatus. Proton and carbon nuclear magnetic resonance (^{1}H and ^{13}C NMR) spectra were recorded in deuterated chloroform ($CDCl_3$) using a Bruker 400 spectrometer (^{1}H at 400 MHz and ^{13}C at 100 MHz). Elemental analyses were performed using a LecoTruspec Micro model instrument. Thermal characterization studies by thermogravimetric analysis (TGA) and differential scanning calorimetry (DSC) were performed under nitrogen at a heating rate of 10 °C min^{-1} using a PerkinElmer Diamond model instrument. Cyclic voltammetry measurements were carried out using a BAS-Epsilon potentiostat/galvanostat from Bioanalytical Systems Inc. (Lafayette, IN) equipped with a C3-cell stand electrochemical station. Working and counter electrodes were Pt, and the reference electrode was Ag/AgCl (3 M NaCl). All the potentials were calibrated with the standard ferrocene/ferrocenium redox couple (Fc/Fc$^+$: $E_{1/2}$ = +0.40 V measured in the current electrochemical set-up). High-resolution mass spectra were measured using a Bruker Microflex LT MALDI-TOF-MS instrument. UV-vis absorption spectra were recorded on a Shimadzu UV-1800 UV-Vis spectrophotometer. The optimization of the molecular geometries and total energy minimizations were obtained by the Gaussian 09 program using density functional theory (DFT) with the B3LYP method and the 6-31G** basis set.[61]

Synthesis and characterization

The synthesis of reference semiconductor molecules **β-DD-TIFDKT** and **β-DD-TIFDKM** was performed in accordance with our previously reported procedures.[25] The synthesis of **IFDK-Br₂** is described in the ESI.†

Synthesis of 2,8-bis((triisopropylsilyl)ethynyl)indeno[1,2-*b*]fluorene-6,12-dione (TIPS-IFDK)

A mixture of 2,8 dibromoindeno[1,2-*b*]fluorene-6,12-dione (**IFDK-Br₂**) (0.500 g, 1.136 mmol), CuI (0.01 g, 0.057 mmol) and Pd(PPh$_3$)$_2$Cl$_2$ (0.079 mg, 0.113 mmol) was dissolved in dry Et$_3$N : DMF (20 ml : 40 mL), and stirred for 5 min. Afterwards, (triisopropylsilyl)acetylene (0.497 g, 2.726 mmol) was added, and the resulting mixture was heated and stirred at 110 °C for 18 h under nitrogen. After completing the reaction, the reaction mixture was allowed to cool down to room temperature, and quenched with water. The reaction mixture was extracted with chloroform, dried with Na$_2$SO$_4$, filtered and concentrated to obtain the crude product as dark red oil. The crude was then purified through column chromatography on silica gel using CHCl$_3$: hexane (2 : 1) as a mobile phase to afford the final product as a pink neon solid (0.467 g, 64% yield). ^{1}H NMR (400 MHz, CDCl$_3$), δ (ppm):

1.15 (s, 42H), 7.50 (d, J = 8.0 Hz, 2H), 7.65 (dd, J = 8.0 Hz, 2H), 7.78 (s, 2H), 7.81 (s, 2H); ^{13}C NMR (100 MHz, CDCl$_3$): δ(ppm): 11.26, 18.66, 93.80, 105.67, 116.37, 120.52, 125.04, 128.05, 133.88, 138.73, 139.59, 142.66, 145.60, 192.01; MS (MALDI-TOF): m/z calcd for C$_{42}$H$_{50}$O$_2$Si$_2$: 642.33 [M]$^+$; found: 643.57 [M + H]$^+$; elemental analysis calcd (%) for C$_{42}$H$_{50}$O$_2$Si$_2$: C 78.45, H 7.84; found: C 78.65, H 7.93.

Synthesis of 2,2′-(2,8-bis((triisopropylsilyl)ethynyl)indeno[1,2-b]fluorene-6,12-diylidene)dimalononitrile (TIPS-IFDM)

A mixture of 2,8-bis((triisopropylsilyl)ethynyl)indeno[1,2-b]fluorene-6,12-dione (TIPS-IFDK) (0.400 g, 0.622 mmol) and malononitrile (0.575 g, 8.71 mmol) was dissolved in dry chlorobenzene (50 mL) under nitrogen, and stirred at 35 °C for 15 min. Afterwards, pyridine (0.935 g, 11.818 mmol) and TiCl$_4$ (1.180 g, 6.22 mmol) were added to the reaction mixture. After addition, the resulting mixture was heated and stirred at 110 °C for 5 h under nitrogen. After completing the reaction, the reaction mixture was allowed to cool down to room temperature, and quenched with water. The reaction mixture was extracted with chloroform, dried with Na$_2$SO$_4$, filtered and concentrated to obtain the crude product as a dark brown solid. The crude was then purified through column chromatography on silica gel using CHCl$_3$: hexane (1 : 1) as a mobile phase to afford the final product as a black solid (0.386 g, 84% yield). ^{1}H NMR (400 MHz, CDCl$_3$), δ (ppm): 1.16 (s, 42H), 7.58 (d, J = 8.0 Hz, 2H), 7.65 (d, J = 8.0 Hz, 2H), 8.49 (s, 2H), 8.56 (s, 2H); ^{13}C NMR (100 MHz, CDCl$_3$): δ (ppm): 11.25, 18.66, 78.98, 95.20, 105.16, 112.40, 118.45, 120.96, 125.63, 130.31, 134.06, 138.64, 139.26, 140.04, 142.98, 158.84; MS (MALDI-TOF): m/z calcd for C$_{48}$H$_{50}$N$_4$Si$_2$: 738.36 [M]$^+$; found: 739.39 [M + H]$^+$; elemental analysis calcd (%) for C$_{48}$H$_{50}$N$_4$Si$_2$: C 78.00, H 6.82, N 7.58; found: C 78.17, H 6.84, N 7.49.

Device fabrication and characterization

For the fabrication of top-contact/bottom-gate (TC/BG) OFETs, highly n-doped silicon wafers with a 300 nm thermally grown SiO$_2$ gate dielectric were used as device substrates. The substrates were cleaned *via* sonication in 2-propanol for 15 min, followed by oxygen plasma cleaning for 5 min (Harrick plasma, PDC-32G, 18 W). A general procedure was employed for PS-brush (M.W. = 19 500 or 28 000 g mol^{-1}) treatment onto the gate dielectric layers.[62–64] Thin films of semiconducting layers were fabricated *via* solution shearing.[56,65,66] During the solution-shearing process, various parameters such as the solvent type (toluene, chlorobenzene, 1,2-dichlorobenzene, and chloroform), semiconductor solution concentration (1–8 mg mL^{-1}), shearing speed (1–8 mm min^{-1}), substrate temperature (~50–65% of the boiling point of the solvent), and thermal annealing temperature (75–85 °C) were optimized. The thicknesses of the semiconductor thin films were measured using a profilometer (DEKTAK-XT, Brucker). The Au electrodes (40 nm) were thermally evaporated under high vacuum (deposition rate = 0.2 Å s^{-1}) yielding various channel lengths (L = 50 and 100 μm) and widths (W = 500 and 1000 μm). The current–voltage characteristics of the fabricated OFETs were measured using a Keithley 4200 SCS at room temperature under vacuum or under ambient atmosphere. The saturation mobility (μ_{sat}) was calculated using the formula:$\mu_{sat} = (2I_{DS}L)/[WC_i(V_G - V_{th})^2]$ where I_{DS} is the source–drain current, L is the channel length, W is the channel width, C_i is the areal capacitance of the gate dielectric, V_G is the gate voltage, and V_{th} is the threshold voltage. The surface morphology and microstructure of thin films were characterized by the atomic force microscopy (AFM, NX10, Park systems) and X-ray diffraction (XRD, D8-Advance, Bruker Miller Co.) techniques, respectively.

Conflicts of interest

There are no conflicts to declare.

Acknowledgements

References

1. H. H. Cho , S. Kim , T. Kim , V. G. Sree , S. H. Jin , F. S. Kim and B. J. Kim , *Adv. Energy Mater.*, 2018, **8** , 1 -8 Search PubMed .

2. P. E. Hartnett , A. Timalsina , H. S. S. Ramakrishna Matte , N. Zhou , X. Guo , W. Zhao , A. Facchetti , R. P. H. Chang , M. C. Hersam , M. R. Wasielewski and T. J. Marks , *J. Am. Chem. Soc.*, 2014, **136** , 16345 -16356 CrossRef PubMed .

3. S. Vegiraju , C. Y. Lin , P. Priyanka , D. Y. Huang , X. L. Luo , H. C. Tsai , S. H. Hong , C. J. Yeh , W. C. Lien , C. L. Wang , S. H. Tung , C. L. Liu , M. C. Chen and A. Facchetti , *Adv. Funct. Mater.*, 2018, **28** , 1 -10 CrossRef .

4. J. Zhang , Y. Li , J. Huang , H. Hu , G. Zhang , T. Ma , P. C. Y. Chow , H. Ade , D. Pan and H. Yan , *J. Am. Chem. Soc.*, 2017, **139** , 16092 -16095 CrossRef PubMed .

5. J. Zhang , H. S. Tan , X. Guo , A. Facchetti and H. Yan , *Nat. Energy*, 2018, 1 -12 Search PubMed .

6. B. Jang , C. Lee , Y. W. Lee , D. Kim , M. A. Uddin , F. S. Kim , B. J. Kim and H. Y. Woo , *Chin. J. Chem.*, 2018, **36**, 199 -205 CrossRef .

7. W. Lee , C. Lee , H. Yu , D. J. Kim , C. Wang , H. Y. Woo , J. H. Oh and B. J. Kim , *Adv. Funct. Mater.*, 2016, **26** , 1543 -1553 CrossRef .

8. X. Guo , Q. Liao , E. F. Manley , Z. Wu , Y. Wang , W. Wang , T. Yang , Y. E. Shin , X. Cheng , Y. Liang , L. X. Chen ,K. J. Baeg , T. J. Marks and X. Guo , *Chem. Mater.*, 2016, **28** , 2449 -2460 CrossRef .

9. M. C. Chen , C. Kim , S. Y. Chen , Y. J. Chiang , M. C. Chung , A. Facchetti and T. J. Marks , *J. Mater. Chem.*, 2008, **18** , 1029 -1036 RSC .

10. P. Leowanawat , A. Nowak-Król and F. Würthner , *Org. Chem. Front.*, 2016, **3** , 537 -544 RSC .

11. A. Nowak-Król , R. Wagener , F. Kraus , A. Mishra , P. Bäuerle and F. Würthner , *Org. Chem. Front.*, 2016, **3** , 545 -555 RSC .

12. X. Guo , A. Facchetti and T. J. Marks , *Chem. Rev.*, 2014, **114** , 8943 -9012 CrossRef PubMed .

13. J. A. Labastide , H. B. Thompson , S. R. Marques , N. S. Colella , A. L. Briseno and M. D. Barnes , *Nat. Commun.*, 2016, **7** , 1 -7 Search PubMed .

14. H. Lee , J. C. Stephenson , L. J. Richter , C. R. McNeill , E. Gann , L. Thomsen , S. Park , J. Jeong , Y. Yi , D. M. DeLongchamp , Z. A. Page , E. Puodziukynaite , T. Emrick and A. L. Briseno , *Adv. Mater. Interfaces*, 2016, **3** , 1 -7 Search PubMed .

15. G.-S. Ryu , Z. Chen , H. Usta , Y.-Y. Noh and A. Facchetti , *MRS Commun.*, 2016, **6** , 47 - 60 CrossRef .

16. J. Hamonnet , M. Nakano , K. Nakano , H. Sugino , K. Takimiya and K. Tajima , *Chem. Mater.*, 2017, **29** , 9618 -9622 CrossRef .

17. S. Kumagai , M. Nakano , K. Takimiya and J. Takeya , *Org. Electron.*, 2018, 10.1016/j.orgel.2018.06.029 Search PubMed .

18. B. D. Rose , D. T. Chase , C. D. Weber , L. N. Zakharov , M. C. Lonergan and M. M. Haley , *Org. Lett.*, 2011, **13** , 2106 -2109 CrossRef PubMed .

19. T. Nakagawa , D. Kumaki , J. I. Nishida , S. Tokito and Y. Yamashita , *Chem. Mater.*, 2008, **20** , 2615 -2617 CrossRef .

20. C. K. Frederickson and M. M. Haley , *J. Org. Chem.*, 2014, **79** , 11241 - 11245 CrossRef PubMed .

21. W. Deuschel *Helv. Chim. Acta*, 1951, **34** , 2403 -2416 CrossRef .

22. C. K. Frederickson , B. D. Rose and M. M. Haley , *Acc. Chem. Res.*, 2017, **50** , 977 - 987 CrossRef PubMed .

23. H. Usta , A. Facchetti and T. J. Marks , *J. Am. Chem. Soc.*, 2008, **130** , 8580 - 8581 CrossRef PubMed .

24. Z. P. Fan , X. Y. Li , X. E. Luo , X. Fei , B. Sun , L. C. Chen , Z. F. Shi , C. L. Sun , X. Shao and H. L. Zhang , *Adv. Funct. Mater.*, 2017, **27** , 1 -10 CrossRef .

25. H. Usta , C. Risko , Z. Wang , H. Huang , M. K. Deliomeroglu , A. Zhukhovitskiy , A. Facchetti and T. J. Marks , *J. Am. Chem. Soc.*, 2009, **131** , 5586 -5608 CrossRef PubMed .

26. M. Ozdemir , D. Choi , G. Kwon , Y. Zorlu , H. Kim , M.-G. Kim , S. Seo , U. Sen , M. Citir , C. Kim and H. Usta , *RSC Adv.*, 2016, **6** , 212 -226 RSC .

27. R. Ozdemir , D. Choi , M. Ozdemir , G. Kwon , H. Kim , U. Sen , C. Kim and H. Usta , *J. Mater. Chem. C*, 2017, **5**, 2368 -2379 RSC .

28. R. Ozdemir , D. Choi , M. Ozdemir , H. Kim , S. T. Kostakoğlu , M. Erkartal , H. Kim , C. Kim and H. Usta , *ChemPhysChem*, 2017, **18** , 850 -861 CrossRef PubMed .

29. M. M. Payne , S. R. Parkin , J. E. Anthony , C. C. Kuo and T. N. Jackson , *J. Am. Chem. Soc.*, 2005, **127** , 4986 -4987 CrossRef PubMed .

30. J. E. Anthony *Chem. Rev.*, 2006, **106** , 5028 -5048 CrossRef PubMed .

31. C. Teixeira da Rocha , K. Haase , Y. Zheng , M. Löffler , M. Hambsch and S. C. B. Mannsfeld , *Adv. Electron. Mater.*, 2018, **1800141** , 1 -9 Search PubMed .

32. A. Naibi Lakshminarayana , A. Ong and C. Chi , *J. Mater. Chem. C*, 2018, **6** , 3551 - 3563 RSC .

33. A. Maliakal , K. Raghavachari , H. Katz , E. Chandross and T. Siegrist , *Chem. Mater.*, 2004, **16** , 4980 -4986 CrossRef .

34. H. Dong , X. Fu , J. Liu , Z. Wang and W. Hu , *Adv. Mater.*, 2013, **25** , 6158 - 6183 CrossRef PubMed .

35. J. W. Ward , Z. A. Lamport and O. D. Jurchescu , *ChemPhysChem*, 2015, **16** , 1118 - 1132 CrossRef PubMed .

36. J. Jiang , B. R. Kaafarani and D. C. Neckers , *J. Org. Chem.*, 2006, **71** , 2155 - 2158 CrossRef PubMed .

37. C. P. Bénard , Z. Geng , M. A. Heuft , K. VanCrey and A. G. Fallis , *J. Org. Chem.*, 2007, **72** , 7229 -7236 CrossRef PubMed .

38. Y. M. Wang , N. Y. Fu , S. H. Chan , H. K. Lee and H. N. C. Wong , *Tetrahedron*, 2007, **63** , 8586 -8597 CrossRef .

39. D. Carmichael , P. Lefloch , X. F. Legoff , O. Piechaczyk and N. Seeboth , *Chem. – Eur. J.*, 2010, **16** , 14486 -14497 CrossRef PubMed .

40. L. Simón and J. M. Goodman , *J. Org. Chem.*, 2010, **75** , 589 -597 CrossRef PubMed .

41. D. Thirion , C. Poriel , J. Rault-Berthelot , F. Barrière and O. Jeannin , *Chem. – Eur. J.*, 2010, **16** , 13646 -13658 CrossRef PubMed .

42. S. Li , M. Aljhdli , H. Thakellapalli , B. Farajidizaji , Y. Zhang , N. G. Akhmedov , C. Milsmann , B. V. Popp and K. K. Wang , *Org. Lett.*, 2017, **19** , 4078 -4081 CrossRef PubMed .

43. J. E. Anthony , D. L. Eaton and S. R. Parkin , *Org. Lett.*, 2002, **4** , 15 -18 CrossRef PubMed .

44. J. E. Anthony , J. S. Brooks , D. L. Eaton and S. R. Parkin , *J. Am. Chem. Soc.*, 2001, **123** , 9482 -9483 CrossRefPubMed .

45. C. D. Sheraw , T. N. Jackson , D. L. Eaton and J. E. Anthony , *Adv. Mater.*, 2003, **15** , 2009 - 2011 CrossRef .

46. L. Zhang , A. Fonari , Y. Liu , A. L. M. Hoyt , H. Lee , D. Granger , S. Parkin , T. P. Russell , J. E. Anthony , J. L. Brédas , V. Coropceanu and A. L. Briseno , *J. Am. Chem. Soc.*, 2014, **136** , 9248 -9251 CrossRef PubMed .

47. D. B. Granger , Y. Mei , K. J. Thorley , S. R. Parkin , O. D. Jurchescu and J. E. Anthony , *Org. Lett.*, 2016, **18** , 6050 -6053 CrossRef PubMed .

48. S. Jung , M. Albariqi , G. Gruntz , T. Al-Hathal , A. Peinado , E. Garcia-Caurel , Y. Nicolas , T. Toupance , Y. Bonnassieux and G. Horowitz , *ACS Appl. Mater. Interfaces*, 2016, **8** , 14701 - 14708 CrossRef PubMed .

49. Y. Nicolas , F. Castet , M. Devynck , P. Tardy , L. Hirsch , C. Labrugère , H. Allouchi and T. Toupance , *Org. Electron. Phys. Mater. Appl.*, 2012, **13** , 1392 -1400 Search PubMed .

50. T. Kato , J. Uchida , T. Ichikawa and T. Sakamoto , *Angew. Chem., Int. Ed.*, 2018, **57** , 4355 - 4371 CrossRefPubMed .

51. H. Iino , T. Usui and J.-I. Hanna , *Nat. Commun.*, 2015, **6** , 6828 CrossRef PubMed .

52. M. Porz , F. Rominger and U. H. F. Bunz , *Cryst. Growth Des.*, 2014, **14** , 5962 - 5965 CrossRef .

53. K. Sbargoud , M. Mamada , T. Jousselin-Oba , Y. Takeda , S. Tokito , A. Yassar , J. Marrot and M. Frigoli , *Chem. – Eur. J.*, 2017, **23** , 5076 -5080 CrossRef PubMed .

54. I. J. Bruno , J. C. Cole , P. R. Edgington , M. Kessler , C. F. Macrae , P. McCabe , J. Pearson and R. Taylor , *Acta Crystallogr., Sect. B: Struct. Sci.*, 2002, **58** , 389 -397 CrossRef .

55. A. Bondi *J. Phys. Chem.*, 1964, **68** , 441 -451 CrossRef .

56. G. Giri , E. Verploegen , S. C. Mannsfeld , S. Atahan-Evrenk , H. Kim do , S. Y. Lee , H. A. Becerril , A. Aspuru-Guzik , M. F. Toney and Z. Bao , *Nature*, 2011, **480** , 504 - 508 CrossRef PubMed .

57. H. A. Becerril , M. E. Roberts , Z. Liu , J. Locklin and Z. Bao , *Adv. Mater.*, 2008, **20** , 2588 - 2594 CrossRef .

58. E. P. K. Currie , W. Norde and M. A. Cohen Stuart , *Adv. Colloid Interface Sci.*, 2003, **100–102** , 205 -265 CrossRef PubMed .

59. P. G. de Gennes *Macromolecules*, 1980, **13** , 1069 -1075 CrossRef .

60. J. Chen , D. C. Martin and J. E. Anthony , *J. Mater. Res.*, 2007, **22** , 1701 -1709 CrossRef .

61. M. J.Frisch, G. W.Trucks, H. B.Schlegel, G. E.Scuseria, M. A.Robb, J. R.Cheeseman, G.Scalmani, V.Barone, B.Mennucci, G. A.Petersson, H.Nakatsuji, M.Caricato, X.Li, H. P.Hratchian, A. F.Izmaylov, J.Bloino, G.Zheng, J. L.Sonnenberg, M.Hada, M.Ehara, K.Toyota, R.Fukuda, J.Hasegawa, M.Ishida, T.Nakajima, Y.Honda, O.Kitao, H.Nakai, T.Vreven, J. A.Montgomery Jr., J. E.Peralta, F.Ogliaro, M.Bearpark, J. J.Heyd, E.Brothers, K. N.Kudin, V. N.Staroverov, R.Kobayashi, J.Normand, K.Raghavachari, A.Rendell, J. C.Burant, S. S.Iyengar,

J.Tomasi, M.Cossi, N.Rega, J. M.Millam, M.Klene, J. E.Knox, J. B.Cross, V.Bakken, C.Adamo, J.Jaramillo, R.Gomperts, R. E.Stratmann, O.Yazyev, A. J.Austin, R.Cammi, C.Pomelli, J. W.Ochterski, R. L.Martin, K.Morokuma, V. G.Zakrzewski, G. A.Voth, P.Salvador, J. J.Dannenberg, S.Dapprich, A. D.Daniels, O.Farkas, J. B.Foresman, J. V.Ortiz, J.Cioslowski and D. J.Fox, Gaussian 09, Revision C.01, Gaussian, Inc., Wallingford CT, 2010.

62. O. Azzaroni *J. Polym. Sci., Part A: Polym. Chem.*, 2012, **50** , 3225 -3258 CrossRef .

63. S. H. Park , H. S. Lee , J.-D. Kim , D. W. Breiby , E. Kim , Y. D. Park , D. Y. Ryu , D. R. Lee and J. H. Cho , *J. Mater. Chem.*, 2011, **21** , 15580 -15586 RSC .

64. S. S. Dharmapurikar , A. Arulkashmir , C. Das , P. Muddellu and K. Krishnamoorthy , *ACS Appl. Mater. Interfaces*, 2013, **5** , 7086 -7093 CrossRef PubMed .

65. Z. Liu , H. A. Becerril , M. E. Roberts , Y. Nishi and Z. Bao , *IEEE Trans. Electron Devices*, 2009, **56** , 176 -185 Search PubMed .

66. Y. Diao , L. Shaw , Z. Bao and S. C. B. Mannsfeld , *Energy Environ. Sci.*, 2014, **7** , 2145 - 2159 RSC .